Analysis of the Discretization Error vs. Estimation Time Tradeoff of MRF Dictionary Matching and the Advantage of the Neural Net-based Approach

Chinmay Rao[1], Jakob Meineke[2], Nicola Pezzotti[3], Marius Staring[1], Matthias van Osch[1], and Mariya Doneva[2]
[1]Leiden University Medical Center, Leiden, Netherlands, [2]Philips Research, Hamburg, Germany, [3]Philips Research, Eindhoven, Netherlands

Synopsis

Traditional MR fingerprinting involves matching the acquired signal evolutions against a dictionary of expected tissue fingerprints to obtain the corresponding tissue parameters. Since this dictionary is essentially a discrete representation of a physical model and the matching process amounts to brute-force search in a discretized parameter space, there arises a tradeoff between discretization error and parameter estimation time. In this work, we investigate this tradeoff and show via numerical simulation how a neural net-based approach solves it. We additionally conduct a phantom study using 1.5T and 3T data to demonstrate the consistency of neural net-based estimation with dictionary matching.

Introduction

Magnetic Resonance Fingerprinting (MRF) [1] is a quantitative MRI technique combining fast data acquisition with robust parameter mapping. One of its key enablers is dictionary-based parameter estimation. An MRF dictionary is a discrete representation of a physical model constructed by grid-sampling the parameter space. Naturally, there comes a tradeoff between grid density and matching speed. In neural network (NN)-based MRF parameter estimation [2-4], a trained NN model represents a continuous functional approximation of the inverse physical model and can, in theory, overcome the fundamental limitation of traditional matching. We show via numerical simulation that the NN-based approach is consistent with full dictionary matching (FDM) and that fast matching at the speed of the NN performed with a reduced dictionary (RDM) produces a predictable worst-case discretization error. Further, to strengthen the former result, we evaluate the agreement between NN and FDM on phantom data acquired using two field strengths.

Methods

We used a sequence of 625 time points, TR=12 ms, TE=3 ms, and an optimized FA pattern [5]. A dictionary of 308922 fingerprints was computed using Bloch simulation for a T_1/T_2 grid with T_1 range 9-5056 ms, T_2 range 5-2018 ms, and 2% grid spacing relative to T_1/T_2 values. The dictionary was compressed in time domain to 6 coefficients using SVD. A 6-layer complex-valued NN [3] was defined that accepts compressed fingerprints and outputs T_1 and T_2 parameters. To simulate realistic signal corruption for training, fingerprints were scaled by a random complex scaling factor with magnitude 0.4-2.4 and phase 0-2π. Complex Gaussian noise of σ=0.01 was added resulting in SNR_{max} range 40-240, where SNR_{max} is defined as the noise level relative to the MR signal from a fully relaxed spin system (with M_0=1) excited by a 90° pulse [6]. The fingerprints were normalized to have unit L_2 norm. The dictionary was randomly split 90%-10% for training and validation. The NN model was trained using Cramér-Rao bound-weighted MSE loss [4] and Adam optimizer (0.001 learning rate, 512 batch-size, 500 epochs). For numerical simulation, first, the estimation time was defined as the time required to compute T_1/T_2 maps given a single-slice image series of size 224x224 and 6 coefficients. On Intel Xeon W-2235 CPU, FDM and NN inference required 23.4 s and 0.5 s, respectively. Then, a coarse dictionary was created with a 36x subsampled T_1/T_2 grid - 6x along each axis - which matched within the same time budget as our NN. We conducted in-dictionary and out-of-dictionary bias-variance analyses where 12 T_1/T_2 combinations were chosen from the reduced dictionary's grid and 12 from halfway between its grid points. In each case, 250 noisy realizations of fingerprints per T_1/T_2 combination were produced at 4 noise levels - SNR_{max}={50,100,150,200}. Estimation bias and variance of FDM, RDM, and our NN were calculated. For the phantom study, four scans of the T_2-plane of an HPD System Phantom Model 130 [7] were acquired using Philips Ingenia 1.5T/3T scanners with 15-channel head coil. All scans were in coronal orientation with 224 mm x 224 mm FOV, 1 mm x 1 mm in-plane resolution, and 4 mm slice thickness. A multi-slice spiral acquisition trajectory (5.9 ms window, 36 interleaves) was used to obtain k-space data for 15 slices. Coefficient images were reconstructed from the non-Cartesian k-space data using a non-iterative low-rank inversion method. For each series, T_1/T_2 maps were estimated for the central slice using FDM and our NN, and their probe-wise distributions were compared.

Results and Discussion

In the in-dictionary simulation scenario (Figure 1), RDM was comparable to FDM at SNR_{max}=50. With increasing SNR, RDM's variance became slightly lower. This can be attributed to the greater noise contribution than the discretization's contribution (which is zero) to the variance. At SNR_{max}≥100, RDM's coarse T_1/T_2 grid offered greater isolation between signal noise and estimate variance resulting in more robust matching. In the out-of-dictionary case (Figure 2), while all three methods were comparable at SNR_{max}=50, RDM approached a fixed 6% standard deviation in higher T_1 and mid-range T_2 values at SNR_{max}≥100. This was expected considering the 6x reduction factor along the T_1 and T_2 grid axes of the reduced dictionary and because the out-of-dictionary T_1/T_2 values represented the worst-case off-grid points for RDM which maximized the contribution of discretization in the estimation variance. Thus, the drawback of RDM in the out-of-dictionary scenario outweighed its advantage in the in-dictionary case. In contrast, our NN was consistent with FDM in each case in terms of variance. In the phantom results (Figures 3, 4, and 5), a high agreement between our NN and FDM was observed for T1 and T2 at both 1.5T and 3T field strengths.

Conclusion

T_1/T_2 estimation using an NN was not only comparable in precision to matching with a dense dictionary but also was 46x faster. To achieve fast matching, the dictionary had to be heavily subsampled by a factor of 36 thereby trading away its precision and demonstrating a fundamental limitation of dictionary matching. Estimation using a simulation-trained NN can replace FDM without significant change in estimation quality for scans of a standardized phantom at multiple field strengths. Future work will investigate the effect of discretization on *in vivo* data where the T_1/T_2 distribution is more heterogeneous.

Acknowledgements

We would like to thank Kay Nehrke and Yoo Jin Lee for their support with data acquisition and pre-processing and Thomas Amthor for his support with the software implementation of the MRF physical model and dictionary matching.

References

1. Ma D et al., Nature. 2013 Mar; 495(7440):187-92.

2. Cohen O et al., Magn Reson Med. 2018 Sep; 80(3):885-94.
3. Virtue P et al., Proc IEEE ICIP. 2017 Sep; (pp. 3953-3957).
4. Zhang X et al., Magn Reson Med. 2022 Jul; 88(1):436-48.
5. Sommer K et al., Magn Reson Imaging. 2017 Sep; 41:7-14.
6. Assländer J, J Magn Reson. 2021 Mar; 53(3):676-85.
7. Stupic KF et al., Magn Reson Med. 2021 Sep; 86(3):1194-211.

Figures

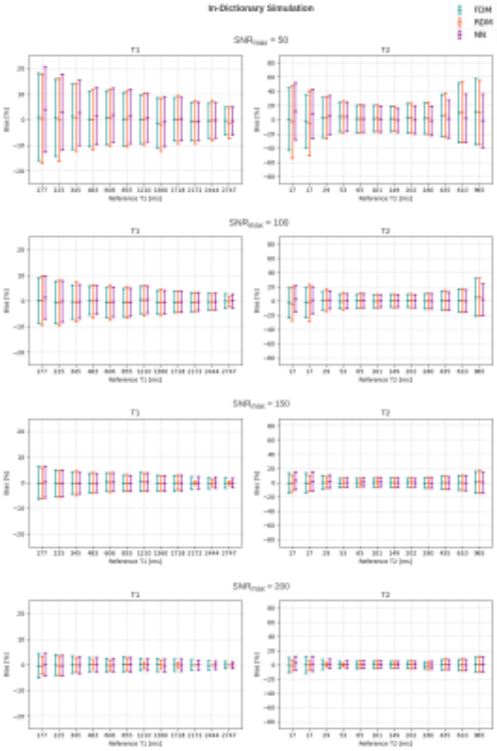

Figure 1: Bias-variance plots of T_1 and T_2 at different SNR_{max} levels for in-dictionary simulation. In each plot, bias is presented relative to the reference parameter value, and confidence intervals represent 1 standard deviation per side.

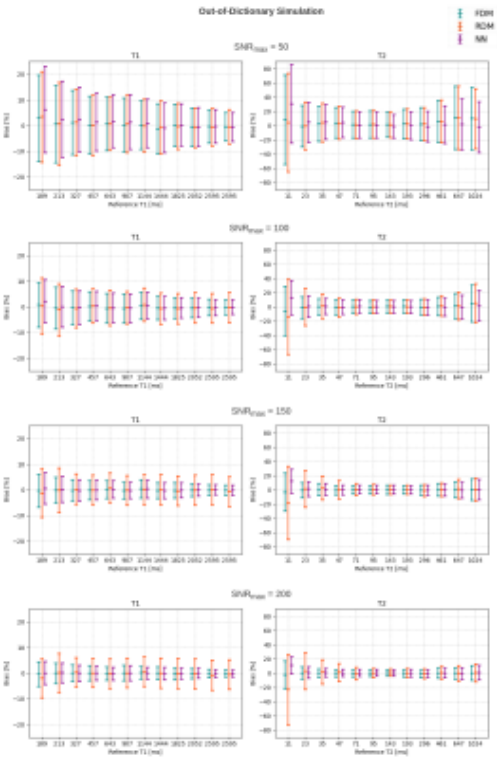

Figure 2: Bias-variance plots of T_1 and T_2 at different SNR_{max} levels for out-of-dictionary simulation. In each plot, bias is presented relative to the reference parameter value, and confidence intervals represent 1 standard deviation per side.

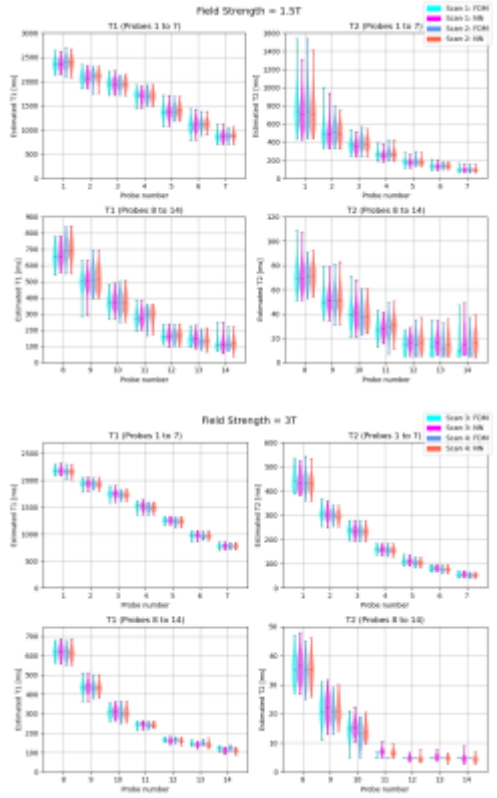

Figure 3: Probe-wise distribution of T_1 and T_2 estimates for 1.5T and 3T phantom data showing comparing NN with FDM. Scans 1 and 2 were acquired with 1.5T scanner whereas scans 3 and 4 with 3T scanner. For better visualization, results corresponding to the phantom's 14 probes are split into two parts - probes 1-7 and 8-14. Bars indicate estimation median and range.

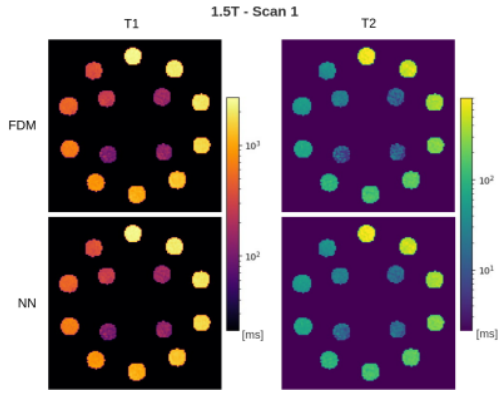

Figure 4: Estimated maps for 1.5T phantom scan 1. Background values are masked away to focus on the probes. Color scales are logarithmic.

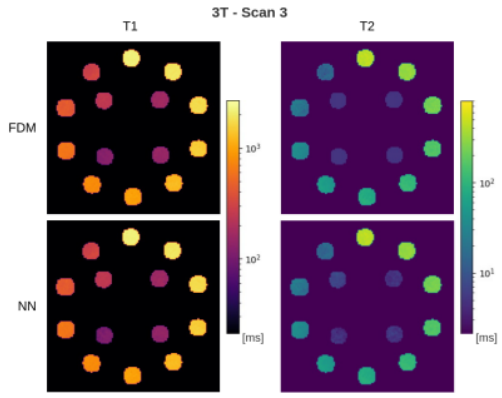

Figure 5: Estimated maps for 3T phantom scan 3. Background values are masked away to focus on the probes. Color scales are logarithmic.